Journal of Molecular Structure 1137 (2017) 97–108

Contents lists available at ScienceDirect

Journal of Molecular Structure

journal homepage: http://www.elsevier.com/locate/molstruc

Structural and vibrational analyses of new potential anticancer drug 2-(phenylmethyl)-2-azaspiro[5.11]heptadecane-1,3,7-trione

Željko J. Vitnik [a, *], Jelena B. Popović-Đorđević [b], Vesna D. Vitnik [a]

[a] Department of Chemistry, Institute of Chemistry, Technology and Metallurgy, University of Belgrade, Studentski trg 12-16, 11001, Belgrade, Serbia
[b] Department of Chemistry and Biochemistry, Faculty of Agriculture, University of Belgrade, Nemanjina 6, 11080, Belgrade, Serbia

ARTICLE INFO

Article history:
Received 12 December 2016
Received in revised form
1 February 2017
Accepted 2 February 2017
Available online 7 February 2017

Keywords:
2-(Phenylmethyl)-2-azaspiro[5.11]heptadecane-1,3,7-trione
Vibrational spectra
NMR spectra
NBO analysis
MEP

ABSTRACT

The establishment of the most stable structures of 2-(phenylmethyl)-2-azaspiro[5.11]heptadecane-1,3,7-trione, potential anticancer and antimicrobial drug has been investigated in this work. A detailed interpretation of experimental and calculated IR, UV and NMR spectra were reported. The equilibrium geometry, harmonic vibrational frequencies and electronic properties have been investigated with Density Functional Theory using B3LYP/6-311++G(d,p) method. The scaled theoretical wavenumber showed very good agreement with the experimental values. The charge transfer in the molecule was confirmed with NBO analysis. Ultraviolet–visible spectrum was calculated using TD-DFT method and compared with experimental spectrum. The calculated energy and oscillator strength well reproduce the experimental data. The molecular electrostatic potential surface map portrays potential binding sites of the title molecule.

1. Introduction

Cyclic imides, especially five- and six-membered systems, are important group of bioactive molecules. They exhibit antitumor (sesbanimide [1], iso-migrastatin [2], lactimidomycin [3]), anti-inflammatory [4], immunomodulatory, antiangiogenic (thalidomide and analogues) [5], and anxiolytic (buspirone [6] and tandospirone [7]) activities.

Isolation and examination of pharmacologicaly active natural glutarimides started in 1960s. It was found that cycloheximide [8] and streptimidone [9–11] act as very potent cytotoxic agents [12,13]. Structurally related natural product lactimidomycin (LTM), 12-membered unsaturated macrolide antibiotic, produced by *Streptomyces amphibiosporus* R310-104 (ATCC 53964), is characterized by a biosynthetically rare glutarimide side chain and display strong *in vitro* cytotoxicity against a number of human tumor cell lines, *in vivo* antitumor activity in mice model, and potent antifungal activity [2].

After extensive research controversial drug thalidomide (α-(*N*-phthalimido)glutarimide) was approved as a drug for treatment of certain cancers (newly diagnosed multiple myeloma) and for complication arrised from leprosy as well as analogues of thalidomide with increased potency, 3-amino-thalidomid (pomalidomid, Pomalyst) and α-(3-aminophthalimido)glutarimide (lenalidomid, Revlimid) have been developed [14,15]. Lenalidomid is used for treatment of multiple myeloma, while pomalidomid is recently approved by FDA for treatment of relapsed and refractory multiple myeloma.

In the past decade, antitumor activity *in vitro* of mitonafide [16], amonafide [17], and naphthalimide [18] derivatives was intensively examined.

In addition, glutarimides have applications in various other fields; for example, they are employed as polymers, activators and stabilizers, vulcanizing agents, lubricant additives, dyes and optical brightening agents, photographic and printing aids [19].

The most typical feature of glutarimide derivatives is that the pharmacological and spectroscopic properties can be readily modified by introduction of substituents in the glutarimide ring. Moreover, we are performing the synthesis and the properties relevant to antiproliferative and antibacterial activities of one series of glutarimide derivatives, with some newly synthesised compounds [20]. Cytotoxicity was tested toward three human cancer cell lines, HeLa, K562 and MDA-MB-453 by MTT assay. Compound 2-(phenylmethyl)-2-azaspiro[5.11]heptadecane-1,3,7-trione (abbreviated as PAH), containing 12-membered ketone ring, was

* Corresponding author.
E-mail address: zvitnik@chem.bg.ac.rs (Ž.J. Vitnik).

http://dx.doi.org/10.1016/j.molstruc.2017.02.012
0022-2860/

found to be the most potent toward all tested cell lines (IC_{50} = 9–27 μM). Also, minimum inhibitory concentration (MIC) determined by broth microdilution method confirmed that compound PAH inhibited the growth of all tested Gram-positive and some of the Gram-negative bacteria.

In this paper we describe our results on 2-(phenylmethyl)-2-azaspiro[5.11]heptadecane-1,3,7-trione (PAH) regarding the conformational, vibrational, electronic, NMR and reactivity analyses through spectral measurements. The vibrational spectra of PAH molecule have been analyzed completely to identify the various normal modes with higher wavenumber accuracy. Density Functional Theory (DFT) B3LYP/6-311++G(d,p) calculations have been performed to support our wavenumber assignments. The natural bond orbital (NBO) analysis has been done to prove the stabilization originating from the hyperconjugation of various intramolecular interactions. The UV-Vis spectroscopic studies along with frontier molecular orbital (FMO) analysis have been used to elucidate charge transfer through the molecule. Additionally, molecular electrostatic potential (MEP) surface is plotted over the optimized geometry to explain the reactivity and potential binding sites of PAH molecule. The calculated results were compared with the experimental and the observed spectra were analyzed in detail.

2. Experimental details

Chemicals and solvents (analytical grade) were purchased from Merck (Darmstadt, Germany), Sigma-Aldrich and Fluka. All solvents were dried by standard methods and distilled before use. The sodium hydride was used as 60% dispersion in mineral oil. The reaction was monitored on silica gel precoated TLC plates, HF_{254} (Merck, Darmstadt, Germany). PAH was synthesised by tandem process described in our previous paper [21]. The process involved base-catalyzed Michael addition of active methylene compound to secondary acrylamide, followed by intramolecular *N*-acylation of the carboxamido group. PAH was synthesised in reaction of methyl-2-oxocyclododecane carboxylate (8.32 mmol), *N*-benzylacrylamide (12.5 mmol), *t*-BuOK (0.47 g, 4.16 mmol) and 18-crown-6 ether (0.3 g, 1.25 mmol) in a mixture of solvents THF/*t*-Pentanol (3:1). The reaction mixture was heated (70 °C, 3 h) and stirred under argon. Purification by dry-flash chromatography (SiO_2, hexane/EtOAc) yielded PAH as white crystals in a yield of 55%. The synthesis of PAH is shown in Scheme S1, Supplementary material.

The chemical structure and purity of the synthesised compound was confirmed by its melting point, ^1H and ^{13}C NMR, FT-IR, UV and ESI/HR-MS spectra. FT-IR spectrum was recorded with a Bomem MB 100 spectrophotometer. FT-IR spectrum of this compound was recorded in the region 400–4000 cm^{-1} at a resolution of 4 cm^{-1}. The ultraviolet absorption spectrum of PAH was recorded from a 10^{-5} molar solution of PAH in chloroform and in the range 200–500 nm, using Shimadzu 1700 UV/Vis spectrophotometer. ^1H and ^{13}C NMR spectra were recorded in $CDCl_3$ using TMS as an internal standard on a Bruker Avance 500 spectrometer at 500 MHz and 125 MHz, respectively. ESI-MS spectra were recorded on Agilent Technologies 6210-1210 TOF-LC-ESI-HR/MS instrument.

3. Computational details

Initial calculations are shown that molecule of PAH can adopt two envelope conformations of glutarimide ring, two conformers accordingly to position of benzyl group and huge number of conformers for 12-membered ring. For generation of conformers for 12-membered ring the AMMP program [22] and Vega ZZ GUI [23] were used. The conformers are generated using the systematically conformational search and minimized with SP4 force field. Trajectories are analyzed, selected geometries are extracted with CatDCD, part of VMD program [24], and re-optimized with PM3 and B3LYP methods using Gaussian 09 program package [25]. All generated geometries are minimized without any constraint in the potential energy surface. The stability of the optimized geometries was confirmed by frequency calculations, which gave positive values for all the obtained frequencies. Optimized structural parameters were used in the vibrational frequency, electronic properties and isotropic chemical shift calculations.

The assignments of the calculated wavenumbers were aided by the animation option of Gauss View 5.0 graphical interface from Gaussian programs. Furthermore, the theoretical vibrational spectra of the title compound are interpreted by means of Potential Energy Distribution (PED) using VEDA 4 program [26]. The harmonic frequencies were calculated with B3LYP/6-311++G(d,p) method and then scaled by 0.9604 [27] because the vibrational frequency values computed at this level contain known systematic errors [28]. The nuclear magnetic resonance (NMR) chemical shifts calculations were performed using Gauge- Independent Atomic Orbital (GIAO) method [29,30] at B3LYP level with 6–311++G(d,p) basis set and the ^1H and ^{13}C isotropic chemical shifts were referenced to the corresponding value for TMS, which was calculated at the same level of theory. The effect of solvent on the theoretical NMR parameters was included using conductor polarizable continuum model (CPCM) [31]. Chloroform ($CHCl_3$) was used as solvent.

UV absorption spectrum of this compound was calculated by TD-DFT method in chloroform solvent. The FMO analysis of PAH was also calculated at the same level of theory. The NBO calculations were performed using NBO 3.1 program [32] as implemented in the Gaussian 09 package at the B3LYP/6-311++G(d,p) level. To portray the bonding sites and investigate chemical reactivity of the title molecule, MEP surface, for the 0.002 a.u. isosurfaces of electron density, is plotted over the optimized geometry of the most stable isomer **I** of PAH using Gauss View 5.0 program.

4. Results and discussion

4.1. Conformational stability

The investigation of the most stable isomer of PAH, the challenging task in conformational analysis, has been studied. Also, the aim of the conformational analysis of the PAH molecule is to provide the best model for the molecular structure.

Molecule of PAH can adopt four conformers according to glutarimide ring and position of benzyl group and huge number of conformations for 12-membered ring. For each of these four conformers the systematically conformational search was done changing the torsion angles around eleven C–C bonds of 12-membered ring for 120° followed by full minimization with SP4 force field. The one of the C–C bonds, which contains spiro C atom, is not included in systematically search to avoid a generation of huge number of unnatural conformers. To retain statistical probability of finding the all relevant conformers, the two searches were done with different C–C (spiro) bonds. The all generated trajectories are analyzed and ~5% of energetically most stable geometries of conformers are extracted and re-optimized with PM3 method. All diverse conformers optimized with PM3 which do not differ in energy from the most stable one for more then 10 kcal/mol were additionally re-optimized with B3LYP/6-31G(d) method. Then the full geometry optimizations of all unique structures were performed by B3LYP method with 6–311++G(d,p) basis set.

As a result of these analyses conformer **I** have been obtained as energetically most stable one and it is shown in Figs. 1 and 2. Fig. 1 also presents the geometries of the fifty stable conformers of PAH (**I**-**L**). The energies of these conformers as well as the relative

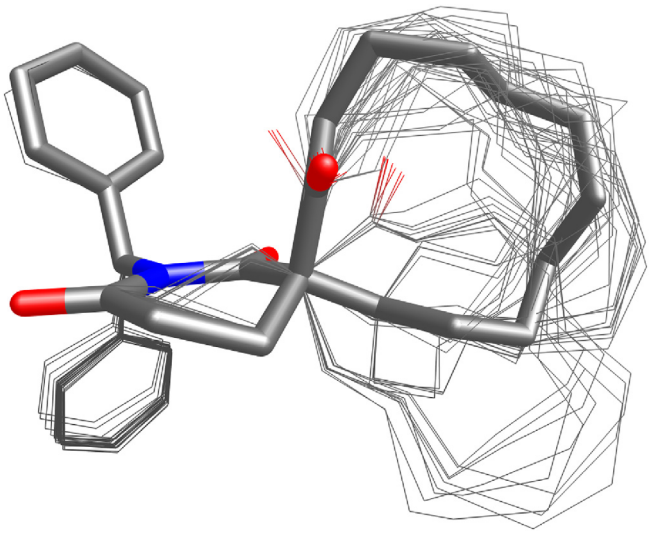

Fig. 1. Superimposed molecular structures of the fifty most stable conformers of 2-(phenylmethyl)-2-azaspiro[5.11]heptadecane-1,3,7-trione. The most stable conformer **I** is presented as tube structure.

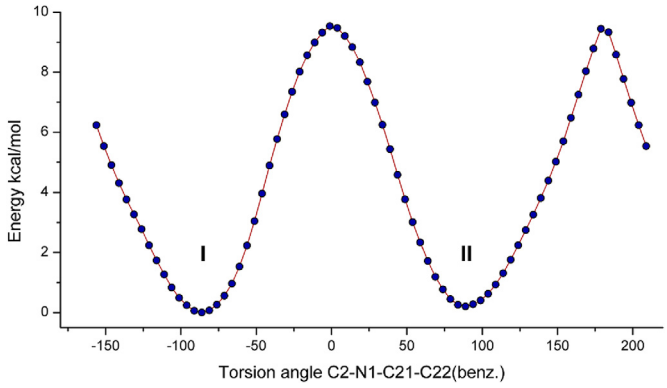

Fig. 3. The potential energy curve of PAH along the C2–N1–C21–C22 dihedral angle.

energies and statistical Boltzmann distribution weighted values, are presented in Table S1 (Supplementary material). From Fig. 1 it can be seen that conformer **I** have glutarimide ring in the envelope conformation with C4 atom under the plane of the glutarimide ring. This position of C4 atom is a prerequisite for the axial position of C3–C7 bond and at the same time the axial position of C7=O10 carbonyl group of cyclododecanone ring. Also, in this conformation, orientation of C7=O10 group is *cis* relative to the benzyl group, namely benzyl group is on the upper side of the plane of glutarimide ring. From Table S1 (Supplementary material), it can be concluded that the energy differences between conformers are low and therefore they can easily convert from one to another under the influence of external interactions.

In order to estimate the barrier height and confirm the transitions between conformers for the rotation around the C–C and N–C bonds potential energy curves are calculated using the B3LYP method with 6-31+G(d) basis set. The potential energy surface (PES) study has been carried out to confirm the orientation of benzyl group in PAH molecule. PES for the rotation of the benzyl group about N1–C21 bond was obtained for molecule **I** by calculating the variation of its total energy with change in the dihedral angle τ(C2–N1–C21–C22) between 0° and 360° in intervals of 5° by B3LYP/6-31 + G(d) calculations. The PES scan for the position of benzyl group of PAH molecule is shown in Fig. 3. For this rotation two minima energy curve have been obtained at −86.13 and 88.83° (conformers **I** and **II**) as shown in Fig. 3 clearly demonstrates that the first minimum corresponds to the most stable conformer **I**. Thus, in its more stable configuration, the benzyl group is in *cis* orientation to the carbonyl group of cyclododecanone ring. It should be noted that the energy difference between these two structures is about 0.2 kcal/mol, which confirms that they can easily convert from one to another.

Also, the PES scan for glutarimide part of investigated molecule is shown in Fig. 4. During the calculation all the geometrical parameters were simultaneously relaxed while the dihedral angles C3–C4–C5–C6 were varied form 60° to −80° by steps of 2.5°. Results of the geometry optimizations indicate that the title compound has two envelop conformers **XI** (−55°) and **I** (50°) for investigated dihedral angles, respectively. However, the latter is

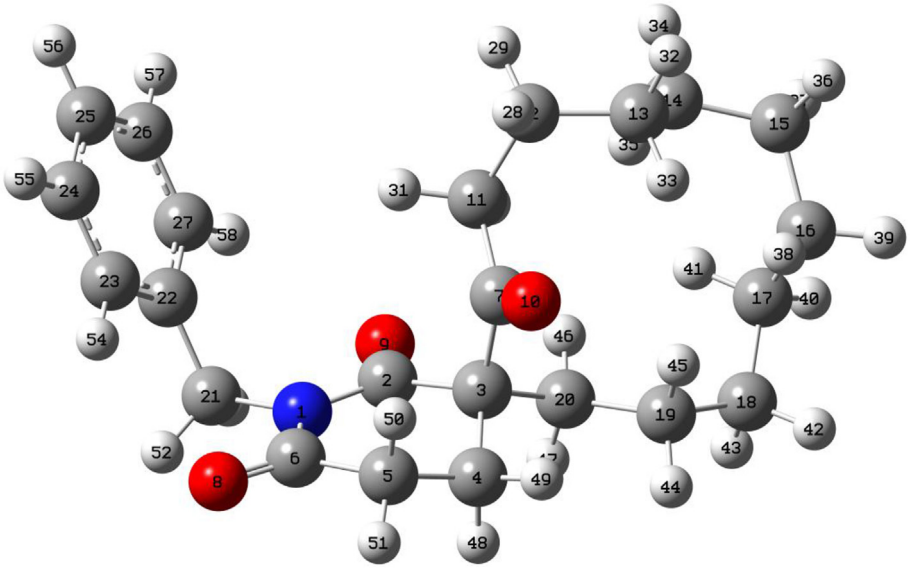

Fig. 2. Optimized molecular structure and atomic numbering of PAH (**I**).

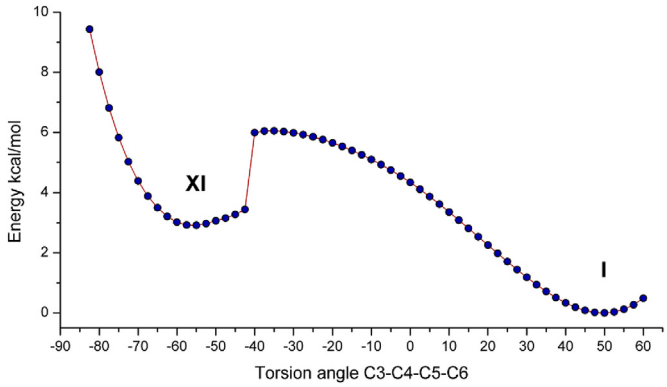

Fig. 4. The potential energy curve of PAH along the C3–C4–C5–C6 dihedral angles.

deeper than the former and represents the more stable conformation. The potential energy surface diagrams reveal that the conformation with minimum energy corresponds to the structure in which C4 atom lies under the plane of the glutarimide ring.

The PES scan for the dihedral angle C14–C15–C16–C17 of cyclododecanone part was varied form 0°–360° by steps of 5°. For this rotation, four minima energy curve have been obtained as shown in Fig. 5. The energy difference between these structures is about 5 kcal/mol and potential energy minimum at 67.4° corresponds to the most stable conformer **I**.

4.2. Molecular geometry

The optimized geometrical parameters of conformer **I** of PAH calculated by B3LYP level with 6–311++G(d,p) basis set are listed in Table S2 (Supplementary material), the atom numbering scheme is given in Fig. 2. There is no X-ray crystal structure for this compound, so the calculated and experimental structural data have not been compared.

4.3. Vibrational analysis

The molecule PAH belongs to C1 point group and possesses 168 normal vibrational modes. The calculated frequencies are slightly higher than the experimental values for almost all of the normal modes. Two factors are responsible for this. The first is caused by the combination of electron correlation effects and basis set deficiencies and the second reason is the fact that the experimental value is an anharmonic frequency while the calculated value is a harmonic frequency. The theoretical harmonic wavenumbers have been scaled by the scale factor of 0.9604 [27]. After implementing scaling procedure, the theoretically computed wavenumbers matched well with the experimental ones. For comparison, scaled theoretical and experimental FT-IR wavenumbers are presented in Table 1 along with vibrational assignments and calculated IR intensities. The experimental and calculated FT-IR spectra are shown in Fig. 6. The detailed assignments along with the percentage of PED are summarized in Table 1, the assignments having <10% (PED percentage) are not presented.

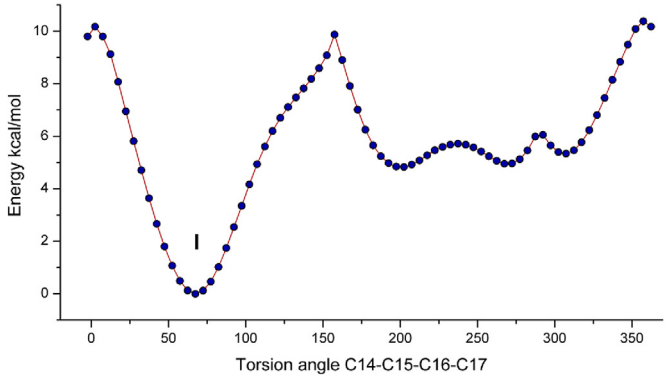

Fig. 5. The potential energy curve of PAH along the C14–C15–C16–C17 dihedral angle.

After scaling, correlation graph which presents the experimental (FT-IR) *vs.* calculated wavenumbers was drawn (Fig. S1, Supplementary material). The relation between these results is linear and described by the equation:

$$\nu_{cal.} = 1.0012\nu_{exp.} - 16.0386\ (R^2 = 0.9996) \text{ for B3LYP/6-311++G(d,p)}$$

Comparison of the wavenumbers calculated by the DFT/B3LYP method using 6-311++G(d,p) basis set with experimental values confirms that this method show good agreement with correlation coefficient 0.9996, Fig. S1 (Supplementary material).

The investigated molecule consists of a glutarimide ring substituted with a cyclododecanone ring at position 3 and a benzyl group at position 1. Consequently, the vibrational modes are discussed in tree parts: vibrations of glutarimide ring, vibrations of benzyl group and vibrations of cyclododecanone group.

4.3.1. Vibrations of glutarimide ring

4.3.1.1. C=O group vibrations. It is well known in the literature that strongly polar bonds such as carbonyl groups produce very strong bands [33]. On the basis of PED, the prominent absorptions at 1673 and 1725 cm^{-1} in FT-IR are assigned to C2=O9 and C6=O8 stretching modes, respectively. The results of computations give the wavenumbers of these modes at 1644 and 1699 cm^{-1}. The region below 800 cm^{-1} is mostly dominated by in-plane and out-of-plane ring vibrations. Also, the C–O in- and out-of-plane vibrations are expected in this region. The C=O in-plane bending modes are mixed with C–N stretching modes and in-plane bending modes of N–C–O group. The bands at 446, 490 and 621 cm^{-1} in FT-IR are assigned to C=O in-plane bending vibrations. The wavenumbers at 439, 486 and 591 cm^{-1} calculated by B3LYP/6-311++G(d,p) show excellent agreement with the experimental data. The C=O out-of-plane vibrations are coupled with out-of-plane ring vibrations and are observed in the region 160–300 cm^{-1} in calculated IR spectrum.

4.3.1.2. C–N and C–C group vibrations. The identification of C–N vibrations is a difficult task, because of the mixing of bending and stretching bands in region of 1000–1500 cm^{-1}. The C–N stretching absorptions assign in the region 1092–1401 cm^{-1} for substituted piperidines [34]. In 1-(4-Chloro-phenyl)-3-phenyl-succinimide, the C–N stretching bands are found to be in the region 1024–1271 cm^{-1} [35]. In the present work, the FT-IR band observed at 1049, 1142, 1164 and 1281 cm^{-1} are assigned to C–N stretching mode. The theoretically calculated values of C–N stretching vibrations in the region 1040–1275 cm^{-1} (mode nos: 91, 84, 82, 69 and 68) coincide with experimental data. The stretching vibration of N1–C21 bond toward benzyl group, assigned at 883 cm^{-1} (FT-IR) is in agreement with calculated frequency at 877 cm^{-1} (mode no: 109). The C–N–C in-plane bending vibration assigned at 531 cm^{-1} (FT-IR) are in agreement with calculated frequencies by B3LYP/6-311++G(d,p) method at 516 cm^{-1} (mode no: 132). The C–N–C out-of-plane bending vibration found at 478 cm^{-1} and correlate well with the computed value at 468 cm^{-1}.

The observed strong bands at 1004 and 1080 cm^{-1} in FT-IR are assigned to C–C stretching modes for glutarimide ring of PAH

Table 1
The observed and calculated vibrational frequencies using B3LYP/6-311++G(d,p) method for PAH [harmonic frequency (cm^{-1}), IR_{int} (km mol^{-1})].

Mode no.	IR exp cm^{-1}	Unscaled B3LYP	Scaled B3LYP	IR Inten[a]	Assignments[b], PED (%)
1	3086	3191	3064	9.77	$\nu_{sym}CH$ (94)
2		3186	3060	10.94	$\nu_{asy}CH$ (93)
3	3067	3180	3054	14.91	$\nu_{asy}CH$ (87)
4		3169	3043	9.47	$\nu_{asy}CH$ (98)
5		3160	3034	0.06	$\nu_{asy}CH$ (87) + $\nu_{asy}CH$ (11)
6		3156	3031	0.31	$\nu_{asy}C21H_2$ (100)
7	3054	3116	2993	9.67	$\nu_{asy}C4H_2$ (64)
8		3115	2992	4.31	$\nu_{asy}C4H_2$ (81)
9	3030	3106	2983	15.4	$\nu_{asy}C5H_2$ (64)
10		3105	2982	1.82	$\nu_{sym}C21H_2$ (64) + $\nu_{asy}C5H_2$ (17)
11	3003	3104	2981	14.03	$\nu_{sym}C21H_2$ (82) + $\nu_{asy}C5H_2$ (14)
12	2981	3093	2971	45.45	$\nu_{asy}CH_2$ (15) + $\nu_{asy}CH_2$ (11) + $\nu_{asy}CH_2$ (33)
13		3091	2968	37.31	$\nu_{asy}CH_2$ (11) + $\nu_{asy}CH_2$ (51)
14	2962	3074	2952	52.88	$\nu_{asy}CH_2$ (62)
15	2941	3069	2947	87.73	$\nu_{asy}CH_2$ (74)
16		3060	2939	32.15	$\nu_{asy}CH_2$ (62)
17	2931	3056	2935	9.48	$\nu_{sym}C5H_2$ (51) + $\nu_{sym}C4H_2$ (19)
18		3047	2926	9.47	$\nu_{sym}CH_2$ (41) + $\nu_{sym}CH_2$ (13) + $\nu_{asy}CH_2$ (13)
19		3046	2925	40.06	$\nu_{asy}CH_2$ (10) + $\nu_{sym}CH_2$ (55)
20		3037	2917	9.97	$\nu_{sym}CH_2$ (79)
21		3035	2915	22.3	$\nu_{sym}C4H_2$ (13) + $\nu_{sym}CH_2$ (40)
22		3033	2913	33.55	$\nu_{sym}CH_2$ (77)
23	2915	3033	2913	34.94	$\nu_{sym}CH_2$ (75)
24		3030	2910	4.71	$\nu_{sym}C4H2$ (16) + $\nu_{sym}CH_2$ (42)
25		3028	2909	22.99	$\nu_{sym}CH_2$ (31) + $\nu_{sym}CH_2$ (39)
26	2903	3027	2907	29.63	$\nu_{sym}CH_2$ (61)
27		3025	2905	18.91	$\nu_{sym}CH_2$ (30) + $\nu_{sym}CH_2$ (13) + $\nu_{sym}CH_2$ (11) + $\nu_{sym}CH_2$ (17)
28	2866	3023	2903	21.4	$\nu_{sym}CH_2$ (82)
29		3015	2895	8.39	$\nu_{sym}CH_2$ (77)
30		3004	2885	28.52	$\nu_{sym}CH_2$ (83)
31	2848	3003	2884	33.38	$\nu_{sym}CH_2$ (83)
32	1725	1769	1699	149.44	νOC (74)
33	1707	1753	1684	123.5	νOC (82)
34	1673	1712	1644	401.9	νOC (79)
35	1607	1644	1578	2.97	νCC (63) + βHCC (21)
36	1561	1623	1559	3.56	νCC (70)
37	1525	1526	1466	13.58	νCC (58) + βHCC (28)
38	1496	1522	1461	25.87	δCH_2 (67)
39		1515	1455	0.46	δCH_2 (59)
40		1512	1452	0.32	δCH_2 (10) + δCH_2 (55)
41	1467	1507	1448	1.41	$\delta C4H_2$ (67)
42		1498	1439	3.64	δCH_2 (61) + δCH_2 (10)
43		1494	1435	2.71	δCH_2 (54)
44		1492	1432	9.08	δCH_2 (61)
45		1488	1430	9.41	δCH_2 (71)
46		1487	1428	1.93	δCH_2 (62)
47		1486	1427	2.7	βHCH (44) + νCC (21)
48	1457	1485	1426	13.12	$\delta C5H_2$ (72)
49		1484	1425	3.92	δCH_2 (60) + δCH_2 (11)
50	1438	1473	1414	26.53	$\delta C21H_2$ (85)
51	1406	1470	1411	10.26	ωCH_2 (83)
52		1410	1354	0.17	ωCH_2 (33)
53		1407	1351	1.41	ωCH_2 (41) + τHCCC (13)
54	1382	1401	1346	29.47	$\omega C21H_2$ (59)
55		1398	1343	0.99	ωCH_2 (11) + τHCCC (42)
56	1352	1390	1335	31.81	$\omega(C4H_2+C5H_2)$ (42)
57		1387	1332	13.85	ωCH_2 (48)
58	1320	1381	1326	13.42	βHCC (18) + $tC21H_2$ (13)
59		1377	1323	0.5	ωCH_2 (29)
60		1376	1321	0.94	βHCC (16) + ωCH_2 (22)
61		1367	1312	5.47	ωCH_2 (34)
62		1364	1310	6.55	βHCC (35) + $tC4H_2$ (14) + $tC5H_2$ (14)
63	1308	1355	1302	2.76	tCH_2 (17)
64		1353	1299	24.85	νCC (22) + βHCC (40)
65	1294	1345	1292	2.91	βHCC (30)
66		1338	1285	0.46	βHCC (13) + βHCC (18) + τHCCC (11)
67		1331	1278	4.09	βHCC (35)
68		1328	1275	156.91	νCC (14) + νNC (14)
69	1281	1326	1273	105.32	νCC (30) + νNC (10)
70		1322	1269	23.85	βHCC (10) + βHCC (19)
71	1259	1308	1256	7.8	βHCC (11)
72		1303	1251	4.33	βHCC (23)
73		1292	1241	6.81	βHCC (19) + τHCCC (10)

(*continued on next page*)

Table 1 (*continued*)

Mode no.	IR exp cm^{-1}	Unscaled B3LYP	Scaled B3LYP	IR Inten[a]	Assignments[b], PED (%)
74	1248	1281	1231	3.36	t(C4H2+C5H2) (33)
75		1270	1219	13.22	βHCC (18) + tCH2 (12)
76	1235	1236	1187	3.32	tCH2 (28)
77		1230	1181	8.6	βHCC (10)
78		1221	1173	5.79	νCC (67) + βHCC (17)
79	1203	1213	1165	13.22	tC5H2 (33)
80	1181	1205	1157	3.22	νCC (20) + βHCC (73)
81		1198	1150	2.64	βHCH (28)
82	1164	1185	1138	73.52	νNC (12) + βHCC (15)
83		1182	1135	2.63	βHCC (10)
84	1142	1177	1130	167.06	νNC (24)
85	1117	1152	1106	2.15	tCH2 (10)
86		1127	1082	11.42	τHCCC (12)
87		1120	1076	1.85	νCC (10)
88	1080	1105	1061	66.84	νCC (13) + βHCC (24) + βCCC (18)
89		1098	1055	0.14	νCC (60)
90		1096	1053	25.59	νCC (10)
91	1049	1083	1040	11.61	νNC (10)
92		1072	1030	1.5	νCC (43)
93		1061	1019	1.75	νCC (10)
94	1031	1056	1014	25.04	νCC (12)
95	1013	1051	1009	8.68	βCCC (38) + νCC (14) + βHCC (16) + βCCC (18)
96		1046	1005	2.56	νCC (22)
97		1035	994	2.6	νCC (44)
98	1004	1024	984	10.98	νCC (12)
99		1018	978	0.08	νCC(42) + βCCC (45)
100		1016	975	3.97	νCC (36)
101		1006	966	2.6	γHCC (73)
102	966	1003	963	52.76	νCC (19)
103		994	955	0.98	γHCC (78)
104	955	986	947	3.08	ρCH2 (10)
105	942	965	927	15.31	ρCH2 (10)
106	927	951	913	14.02	γHCC (15) + τHCNC (33)
107		939	901	7.55	νCC (11)
108		926	890	1.02	νCC (10)
109	883	914	877	2.22	νNC (11)
110	863	880	845	1.55	ρC5H2 (16)
111	849	877	842	6.12	ρ(C4H2 + C21H2) (10)
112		868	834	1.99	νCC (38)
113	835	864	830	0.78	γHCC (97)
114		839	806	7.46	ρCH2 (10)
115	819	838	805	2.13	νCC (11) + νCC (17) + βCCN (15) + τHCCC (16)
116		815	783	5.1	νCC (16)
117	804	807	775	1.33	ρCH2 (27)
118		795	763	1.85	νCC (22)
119	744	772	742	13.61	γHCC (41)
120	731	765	735	1.55	γOCNC (33)
121		742	713	3.27	τHCCC (12) + τHCCC (10)
122	708	731	702	18.06	ρCH2 (10) + ρCH2 (32)
123		714	686	52.16	τHCCC (10) + τHCCC (31) + τHCCC (35)
124		710	682	12.31	βCCC (10) + γOCCC (24)
125		704	676	4.29	τHCCC (53)
126	662	677	651	18.98	γOCCC (26)
127	637	639	614	13.59	βCCN (10) + γOCCC (14)
128		636	611	0.11	βCCC (85)
129	621	616	591	7.06	νNC (10) + βCCO (10)
130		610	586	17.04	βCCO (23)
131	553	566	543	3.8	τHCCN (16) + γOCCC (17)
132	531	537	516	3.79	νNC (16) + βCCO (16) + βCNC (15)
133		523	503	1.91	βCCC (12)
134	490	506	486	16.83	βCCO (21) + βCCC (12)
135	478	488	468	10.36	γCCC (12) + γCNC (15) + τCNCC
136	465	471	452	3.25	γCCO (13)
137	446	457	439	5.04	νNC (10) + βCCO (23) + βNCO (11)
138	427	430	413	14.2	βCNC (44) + τHCCC (12)
139		416	399	3.51	βCCC (21)
140		415	399	0.51	γCCC (16) + τCCCC (71)
141		405	389	13.3	βCCC (13) + βCCO (10) + βCNC (13)
142		382	367	0.35	βCCC (11) + τCCCC (11)
143		365	350	0.17	βCCC (11) + βCCC (15)
144		339	326	0.47	γCCCC (10)
145		316	303	4.12	γCCCO (16)
146		300	288	6.32	γCNC (12)
147		282	271	0.19	τCCCC (11)
148		278	267	1.22	γCCCC (12)

Table 1 (*continued*)

Mode no.	IR exp cm^{-1}	Unscaled B3LYP	Scaled B3LYP	IR Inten[a]	Assignments[b], PED (%)
149		268	257	1.29	βCCC (21) + τHCCC (13) + τCCCC (22)
150		254	244	0.5	νCC (24) + βCCC (25)
151		250	240	1.57	βCCC (34)
152		226	217	0.1	βCCC (36) + βCCC (11)
153		216	208	0.76	βCCC (20)
154		198	191	0.68	γCNC (25)
155		184	177	2.76	τHCCC (15) + τCCCN (12)
156		183	175	0.43	τCCCC (24)
157		177	170	1.63	βCCC (10) + βCCC (11) + βCCC (12)
158		160	154	5.34	τCCCC (15) + τCNCC (11)
159		134	129	2.64	τCCCC (31)
160		109	105	4.08	τCCCC (14) + τCCCN (13)
161		95	91	0.92	τCCCC (26)
162		82	79	1.83	τCCCC (11)
163		73	70	0.33	βCCC (13) + τCCCC (19)
164		62	59	0.36	γCCCC (26)
165		41	40	0.49	βCCN (11) + τCCCN (11) + τCNCC (20)
166		34	32	0.29	γCCCN (51)
167		26	25	0.04	γCCCN (65)
168		16	15	0.06	τCNCC (66)

[a] IR_{Int} – IR intensity; km mol^{-1}.
[b] PED less than 10% are not shown; ν–stretching; ν_{sym} symmetric stretching; ν_{asy}–asymmetric stretching; β–in plane bending; γ–out-of-plane bending; τ–torsion, ω–wagging; t–twisting; δ–scissoring; ρ–rocking.

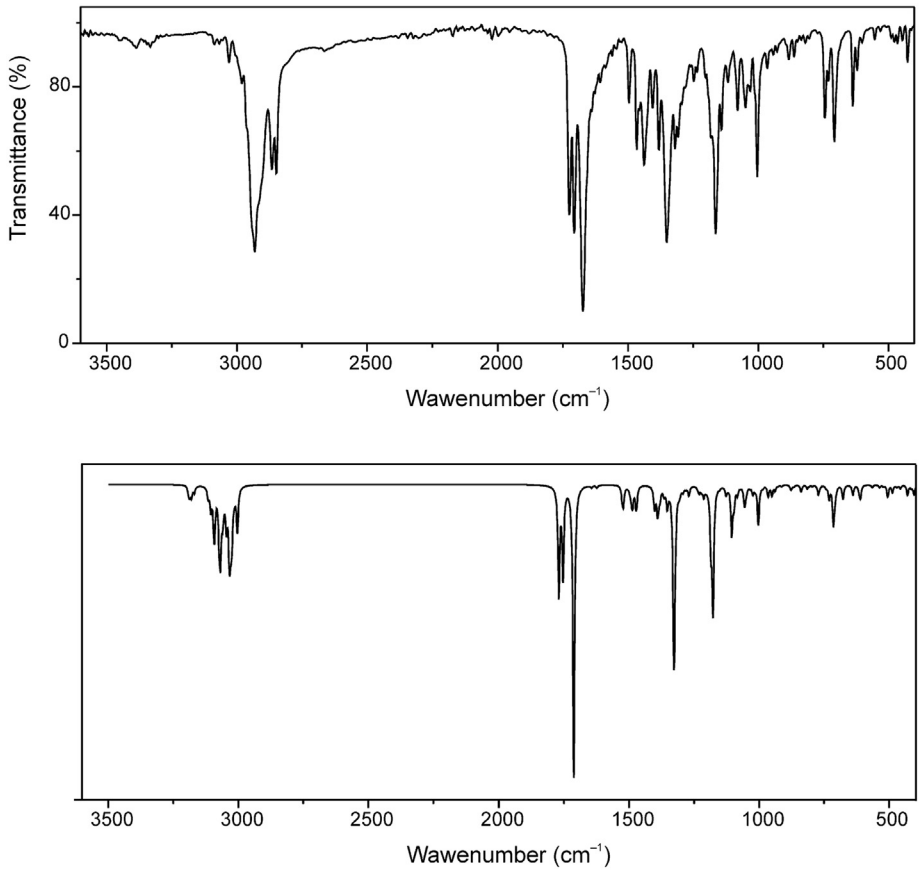

Fig. 6. Comparison of experimental (top) and scaled theoretical IR spectra of PAH.

molecule. The wavenumbers at 984 and 1061 cm^{-1} (mode nos: 98 and 88) calculated by B3LYP/6-311++G(d,p) show excellent agreement with the experimental data. Almost the C–C stretching vibrations are found overlapped with other vibrations and difficult to be assigned. Thus the C–C stretching mode 88 is coupled with in-plane bending C–H and C–C vibrations. However, the mode 97 is pure mode and the PED contribution to this mode is 44%. The C–C–C bending modes are coupled with in-plane bending C–C–O vibrations for glutarimide ring. In FT-IR, band at 490 cm^{-1} is designated as C–C–C in-plane bending modes. The calculated counterparts belong to C–C–C in-plane vibrations are observed in the region 486–611 cm^{-1}. In the present work, the calculated

theoretical wavenumbers 267 and 326 cm^{-1} depicted in Table 1 are assigned as C–C–C out-of-plane vibrations.

4.3.1.3. $C4H_2$ and $C5H_2$ group vibrations. The C–H stretching vibrations of the methylene group are at lower frequencies than those of the aromatic C–H ring stretching. The asymmetric CH_2 stretching vibrations generally observed in the region is 3000–2900 cm^{-1}, while the CH_2 symmetric stretching vibrations are between 2900 and 2800 cm^{-1} [34].

The CH_2 asymmetric and symmetric stretching vibrations of $C4H_2$ and $C5H_2$ group are observed in FT-IR spectrum as weak intensity bands as seen in Table 1 for our title molecule. The band at 2931 cm^{-1} in FT-IR spectrum is assigned to CH_2 symmetric stretching vibrations, for both $C4H_2$ and $C5H_2$ groups. The theoretically computed wavenumbers for these groups are in the range 2910–2935 cm^{-1} (mode nos. 24, 21 and 17). The weak intensity bands at 3030 and 3054 cm^{-1} in FT-IR spectrum are attributed to CH_2 asymmetric stretching vibrations, for $C5H_2$ and $C4H_2$ group, respectively, as shown in Table 1 and correlate well with the calculated values at 2983 and 2993 cm^{-1}, for $C5H_2$ and $C4H_2$ group, respectively.

The fundamental bending CH_2 vibrations of PAH appear in the frequency region 800–1500 cm^{-1}. These vibrations revealed to be mixed with C–C and C–N stretching as well as with C–C–C bending vibrations of glutarimide ring. In FT-IR spectrum of PAH, the weak bands at 1438–1496 cm^{-1} assigned to scissoring vibrations of CH_2 groups. The theoretical wavenumber of CH_2 scissoring vibrations 1426 and 1448 cm^{-1} (mode nos: 48 and 41) coincide very well with experimental values at 1457 and 1467 cm^{-1} for $C5H_2$ and $C4H_2$ unit, respectively. The FT-IR wagging mode at 1352 cm^{-1} corresponding to $C5H_2$ and $C4H_2$ units was calculated to be at 1335 cm^{-1} (mode no: 56). In the present work, the FT-IR frequencies observed in the range 1203–1248 cm^{-1} have been assigned to CH_2 twisting vibrations. The theoretically computed values in the range 1165–1231 cm^{-1} (mode nos: 79, 76 and 74) show excellent agreement with experimental data. The CH_2 rocking vibrations calculated to be 842 and 845 cm^{-1} (mode nos: 111 and 110) are also in excellent agreement with recorded values at 849 and 863 cm^{-1}.

4.3.2. Vibrations of benzyl group

Vibrations of benzyl group are composed of phenyl group and $C21H_2$ group vibrations.

4.3.2.1. Vibrations of phenyl group. Aromatic C–H stretching vibrations generally occur in the region 3000–3100 cm^{-1} [35]. The theoretical description for this region is somewhat difficult due to the weakness of C–H stretching modes. For PAH, the C–H stretching aromatic ring vibrations predicted at 3034–3064 cm^{-1} for B3LYP/6-31++G(d,p) level of theory. These vibrations observed experimentally at 3067–3086 cm^{-1} in the FT-IR spectrum for PAH. The asymmetric stretching vibration of phenyl group is observed as low intense band at 3067 cm^{-1}, while the symmetric stretching vibration is observed at 3086 cm^{-1} in the experimental spectra. The scaled theoretical values at B3LYP/6-311++G(d,p) of aromatic ring C–H stretching modes coincide well with that of experimental data as depicted in Table 1. The percentage of PED predicts that C–H modes of PAH are very pure. The benzene ring C–H in-plane bending vibrations are usually medium and observed in the region 1035–1558 cm^{-1}, while the C–H out-of-plane bending vibrations lie in the region 702–928 cm^{-1} [35]. In-plane C–H bending vibrations of phenyl group are observed in the range of 1164–1607 cm^{-1} and out-of-plane bending vibrations at 744–927 cm^{-1} region, for PAH in the FT-IR spectrum. The in-plane C–H bending vibrations of phenyl group are observed as medium intense bands at 1164, 1181, 1320, 1525 and 1607 cm^{-1} in FT-IR and the corresponding calculated value are 1138, 1157, 1326, 1466 and 1578 cm^{-1}. In-plane C–H bending vibration are also observed at 1173 and 1299 cm^{-1} in calculated IR spectrum which are mixed with stretching C–C vibrations of phenyl group. The weak IR bands at 744, 835 and 927 cm^{-1} are identified as C–H out-plane bends of phenyl ring and the corresponding calculated values are 742, 830 and 913 cm^{-1}. The theoretical wavenumbers of C–H in-plane and out-of-plane are well supported with those of the experimental ones.

The phenyl ring C–C stretching vibrations usually occur in the region 1421–1625 cm^{-1} [36]. The assignment of the skeletal C–C stretching modes in FT-IR is quite difficult, since these bands are masked by the more intense bands at 1200–1600 cm^{-1} originating from the CH_2 deformation vibrations. In the present work, phenyl ring C–C stretching vibrations are observed at 1281, 1525, 1561, and 1607 cm^{-1}, in accordance with the computed values at 1273, 1466, 1559 and 1578 cm^{-1} (mode nos: 69, 37, 36 and 35), respectively. In the present study, the bands observed at 1013 and 1080 cm^{-1} in FT-IR are assigned to ring in-plane bending modes for phenyl group, and the corresponding calculated values are 1009 and 1061 cm^{-1} (mode nos: 95 and 88). The ring out-of-plane bending mode wavenumber is observed at 478 cm^{-1} in FT-IR spectrum and correlate well with the corresponding calculated value at 468 cm^{-1}.

4.3.2.2. $C21H_2$ group vibrations. The methylene group $C21H_2$ have two stretching and the couple of scissoring, wagging, rocking and twisting modes. The symmetric stretching band of this group is observed at 3003 cm^{-1} and correlated well with the theoretically scaled frequencies at 2981 and 2982 cm^{-1}. The asymmetric stretching band of $C21H_2$ group is calculated at 3031 cm^{-1}. The CH_2 scissoring mode generates band at 1438 cm^{-1} in FT-IR is matched well with predicted value at 1414 cm^{-1}. The medium strong band at 1382 cm^{-1} in FT-IR is attributed to CH_2 wagging and correlate well with calculated value at 1346 cm^{-1}. For $C21H_2$ group of the compound, the peaks at 849 and 1320 cm^{-1} in FT-IR are ascribed to rocking and twisting vibrations and the corresponding calculated values are 842 and 1326 cm^{-1}, respectively.

4.3.3. Vibrations of cyclododecanone group

4.3.3.1. C7=O10 group vibrations. The carbonyl stretching wavenumber of C7=O10 group of cyclododecanone ring of PAH is observed at 1707 cm^{-1}. The results of computations give the wavenumber of this mode at 1684 cm^{-1} (mode no. 33). Compared with the C6=O8 group, this group has lower stretching frequency (shift for 18 cm^{-1} to lower wavenumber), but it is underestimated to the stretching frequency of C2=O9. It is well known from the literature that the most intensive peak in the spectrum of cyclododecanone is the C=O stretching which is observed at 1713 cm^{-1} [37]. Also, the very strong intense bands observed in the region 1711–1715 cm^{-1} can be assigned to C=O stretching vibrations in FT-IR spectra of derivatives of cyclododecanone [38]. The vibrational spectrum shows a medium intensive band around the 600 cm^{-1}. The C7–O10 in-plane deformations are observed at 490, 531 and 621 cm^{-1}, respectively and these results are in according with calculated values at 486, 516 and 591 cm^{-1}. The out-of-plane deformation of this carbonyl group is observed at 465 cm^{-1} and calculated value is 452 cm^{-1}.

4.3.3.2. CH_2 group vibrations. As can be seen from Table 1, there are two asymmetric and four symmetric CH_2 stretching vibrations of aliphatic CH_2 groups of cyclododecanone moiety. The asymmetric stretching bands of methylene hydrogens (CH_2) are observed in region 2941–2981 cm^{-1}. The corresponding calculated values are in the region 2939–2971 cm^{-1}. The symmetric stretching bands of

methylene hydrogens are observed at 2848, 2866, 2903 and 2915 cm^{-1} and correlate with the calculated values in the region 2884–2926 cm^{-1}. The fundamental CH_2 vibrations are able to scissoring, wagging, twisting and rocking appear in the frequency region 700–1400 cm^{-1} [39]. In title molecule, the scaled vibrational frequencies in the range of 1461–1428 cm^{-1} (mode nos. 38-46) are assigned to scissoring modes of methylene groups of cyclododecanone moiety are in good agreement with experimental value at 1496 cm^{-1}. The CH_2 wagging mode generate band 1406 $cm^{-1}$and the scaled calculated wagging modes are in the range 1332–1411 cm^{-1}, Table 1. Methylene twisting vibration (tCH_2) of cyclododecanone ring has medium strong peak at 1235 cm^{-1} in FT-IR and is consistent with calculated values in the range 1187–1219 cm^{-1}. Four bands assigned to the rocking vibrations of methylene units are observed at 708, 804, 942 and 955 cm^{-1} and the calculated value are 702, 775, 927 and 947 cm^{-1}.

4.3.4. C–C–C group vibrations

The C–C–C stretching vibrations of cyclododecanone ring predicted at 890–1076 cm^{-1} correlate well with experimentally observed at 966, 1004, 1013, 1031 and 1080 cm^{-1}. The observed frequency at 490 cm^{-1} belongs to the C–C–C in-plane bending mode and the appropriate calculated frequency is 486 cm^{-1} (mode no: 134). In the present work the C–C–C out-of-plane bending mode are calculate at 267 cm^{-1} (mode no: 148).

4.4. Natural bond orbital analysis

The NBO analysis has been performed on PAH molecule in order to explain and confirm intramolecular charge transfer (ICT) and the electron density delocalization within the investigated molecule. The most significant interactions between 'filled' (donor) Lewis type NBO orbitals and 'empty' (acceptor) non Lewis NBO orbitals of PAH molecule are given in Table 2.

In PAH the intramolecular interactions are formed by the orbital overlap between bonding C–C, C–N and antibonding C–C, C–N and C–O orbitals which results in ICT causing stabilization of the PAH molecule. The intramolecular hyperconjugative interaction of the σ orbital of C–C and C–N bonds to the antibonding orbital of C–C and C–N bonds of the glutarimide ring leads to stabilization of the PAH molecule with the stabilization energy in the range of 0.56–2.08 kcal/mol, as evident from Table 2. The intramolecular hyperconjugative interaction of σ(N1–C2) distribute to σ*(N1–C6, N1–C21, C3–C20, C6–O8 and C2–O9) leads to stabilization of 0.56–1.78 kcal/mol. The same kind of interaction is calculated in the distribution from σ(N1–C6), to σ*(N1–C2, N1–C21 and C2–O9) with stabilization energy in the range of 0.97–2.08 kcal/mol. From Table 2 it can be concluded that the bonds in glutarimide ring have electron density of 1.986 e, demonstrating strong delocalization in this part of molecule. The highest σ electron delocalization originates from C2–C3, C5–C6 and N1–C2 bonds of the glutarimide ring with E(2) value in the range 1.16–2.57 kcal/mol. The similar results of σ electron delocalization in cyclododecanone ring are found around σ(C–C) bonds of this ring. NBO analysis obviously manifests the evidences of ICT from σ(C3–C20) to σ*(C3–C7, C7–O10, C18–C19 and C19–C20) orbitals with moderate stabilization energy of 0.57–1.33 kcal/mol, Table 2. Also the results of NBO analysis indicate that strong interaction exists between benzyl group and glutarimide ring. For example, the intramolecular hyperconjugative interaction of σ(N1–C21) distribute to σ*(N1–C2, N1–C6, C2–C3 and C5–C6) leading to stabilization of 0.91–2.57 kcal/mol.

The second order perturbation theory analysis of Fock matrix in

Table 2
Second order perturbation theory analysis of Fock matrix in NBO basis.

Donor NBO (*i*)	Type	ED (*i*) (e)	Acceptor NBO (*j*)	Type	ED (*j*) (e)[a]	E(2)[b] kcal/mol	E(*j*)-E(*i*)[c] a.u.	F(*i*,*j*)[d] a.u.
N1-C2	σ	1.98615	N1-C6	σ*	0.09366	1.12	1.21	0.034
N1-C2	σ		N1-C21	σ*	0.04163	1.01	1.12	0.03
N1-C2	σ		C2-O9	σ*	0.01331	0.56	1.4	0.025
N1-C2	σ		C3-C20	σ*	0.02287	0.75	1.17	0.027
N1-C2	σ		C6-O8	σ*	0.01215	1.78	1.42	0.045
N1-C6	σ	1.98613	N1-C2	σ*	0.08661	1.16	1.21	0.034
N1-C6	σ		N1-C21	σ*	0.04163	0.97	1.11	0.03
N1-C6	σ		C2-O9	σ*	0.01331	2.08	1.39	0.048
C3-C20	σ	1.96225	C3-C7	σ*	0.08676	0.95	0.93	0.027
C3-C20	σ		C7-O10	σ*	0.01446	0.95	1.2	0.03
C3-C20	σ		C18-C19	σ*	0.01391	1.33	0.99	0.033
C3-C20	σ		C19-C20	σ*	0.01511	0.57	0.99	0.021
N1-C21	σ	1.97911	N1-C2	σ*	0.08661	1.08	1.12	0.032
N1-C21	σ		N1-C6	σ*	0.09366	0.91	1.11	0.029
N1-C21	σ		C2-C3	σ*	0.06963	2.57	1.08	0.048
N1-C21	σ		C5-C6	σ*	0.05321	2.09	1.11	0.043
C22-C27	π	1.65538	C23-C24	π*	0.31852	20.41	0.28	0.068
C22-C27	π		C25-C26	π*	0.33228	20.23	0.28	0.067
C23-C24	π	1.65994	C22-C27	π*	0.34826	20.54	0.29	0.068
C23-C24	π		C25-C26	π*	0.33228	20.78	0.28	0.068
C25-C26	π	1.66437	C22-C27	π*	0.34826	20.49	0.29	0.069
C25-C26	π		C23-C24	π*	0.31852	19.72	0.28	0.067
N1	LP (1)	1.60913	C2-O9	π*	0.2328	49.67	0.27	0.109
N1	LP (1)		C6-O8	π*	0.22184	46.83	0.28	0.107
O8	LP (2)	1.86582	N1-C6	σ*	0.09366	27.84	0.66	0.122
O8	LP (2)		C5-C6	σ*	0.05321	17.62	0.65	0.098
O9	LP (2)	1.86776	N1-C2	σ*	0.08661	26.86	0.67	0.121
O9	LP (2)		C2-C3	σ*	0.06963	18.77	0.63	0.099
O10	LP (2)	1.87878	C3-C7	σ*	0.08676	22.59	0.61	0.106
O10	LP (2)		C7-C11	σ*	0.06112	19.02	0.67	0.102

[a] ED, electron density.
[b] E(2) means energy of hyperconjugative interactions.
[c] Energy difference between donor and acceptor *i* and *j* NBO orbitals.
[d] F(*i*,*j*) is the Fock matrix element between *i* and *j* NBO orbitals.

Table 3
Experimental and calculated absorption wavelength λ (nm), excitation energies E (eV), oscillator strengths (*f*) of the most significant singlet excited states for PAH calculated with B3LYP/6-311++G(d,p) method.

Transition	Experimental λ (nm)	TD(DFT) method $CHCl_3$		
		λ (nm)	Excitation energy E (eV)	Oscillator strength *f*
I	340	291.05	5.2599 (98 → 101)	0.0061
II	285	239.57	5.1752 (100 → 102)	0.01
III		234.07	5.2969 (96 → 101)	0.0227

NBO basis of PAH (Table 2) also points out intramolecular interaction due to the orbital overlap of π(C–C) and π*(C–C) of phenyl group, resulting in high electron density (approx. 0.335 e) of anti-bonding π orbitals (C–C).

The interaction energy, related to the resonance in the molecule, is electron withdrawing to the ring through σ*of N1–C6 and C5–C6 bonds from the lone pair LP(2)O8 which leads to stabilization energy of 27.84 and 17.62 kcal/mol, respectively. Also, the magnitude of charge transfer from the lone pairs of LP(2)O9 atom to anti-bonding σ orbitals C2–C3 and N1–C2 of glutarimide ring, amount to stabilization of 18.77 and 26.86 kcal/mol, while from LP(2)O10 to anti-bonding σ orbitals C7–C11 and C3–C7 of cyclododecanone ring is of 19.02 and 22.59 kcal/mol, respectively. The interaction energies of LP(1)N1 → π*(C2–O9) and LP(1)N1 → π*(C6–O8) are 49.67 and 46.83 kcal/mol, respectively. These results additionally confirm the existence of ICT in the investigated molecule.

4.5. Electronic properties

The electronic absorption spectrum of the title compound in chloroform solvent was recorded within the 200–500 nm range and the representative spectrum of computed transitions plot on the experimental is shown in Fig. S2 (Supplementary material). The electronic absorption spectrum of PAH was calculated by the TD-DFT on the B3LYP/6-311++G(d,p) level. The solvent effect was calculated with CPCM method [31]. The calculated vertical excitation energies, wavelength (λ), oscillator strength (*f*), composition of the most significant singlet excited states and experimentally obtained wavelengths are shown in Table 3.

The structure of PAH allow σ–σ* and π–π* transition in the UV-Vis spectrum. NBO analysis indicates that most of molecular orbitals are σ type orbitals, so the electronic transitions are mainly derived from the contribution of σ–σ* bands. However, NBO analysis shows that the electronic transitions derived from π–π* orbitals are dominant and stronger (higher E(2) values, Table 2). The TD-DFT calculation predicts one low intense electronic transition at 291.05 nm with an oscillator strength $f = 0.0061$ which is in good agreement with the experimentally obtained maximum with $\lambda_{exp} = 340$ nm in chloroform, Fig. S2 (Supplementary material). The first transition is between HOMO-2 (orbital 98) and LUMO (orbital 101). The next transition is HOMO (orbital 100) to LUMO+1 (orbital 102) at 239.57 nm, with oscillation strength of 0.01 which correlates well with experimentally found peak at 285 nm, Table 3.

The frontier orbitals, HOMO and LUMO illustrate the way the molecules interact with other species. Therefore, FMO analysis helps to elucidate the chemical reactivity of molecules.

The lowest unoccupied molecular orbital is localized mainly on glutarimide ring and on the part C20–C3–C11 of cyclododecanone ring as shown in Fig. 7. The highest occupied molecular orbital is spread over the benzyl group, imide group of glutarimide ring and the carbonyl group C7=O10. The HOMO (orbital 100) to LUMO (orbital 101) transition implies an electron density transfer to the cyclododecanone ring from the benzyl and imide groups (π → π* transition) and from the lone pair on nitrogen and oxygen atoms (n → π* transition). The HOMO laying at −6.97311 eV and the LUMO laying at −1.45873 eV (computed by TD-DFT) and the energy gap is 5.51 eV.

4.6. NMR analysis

It is well known that chemical shifts of hydrogen and carbon atoms in NMR spectra contain information about the molecular structure. Also, the chemical shifts show sensitivity according to conformational variations. The combination of experimental and computational NMR spectra is used to prove the structure of the most stable isomer of PAH molecule. The experimental NMR

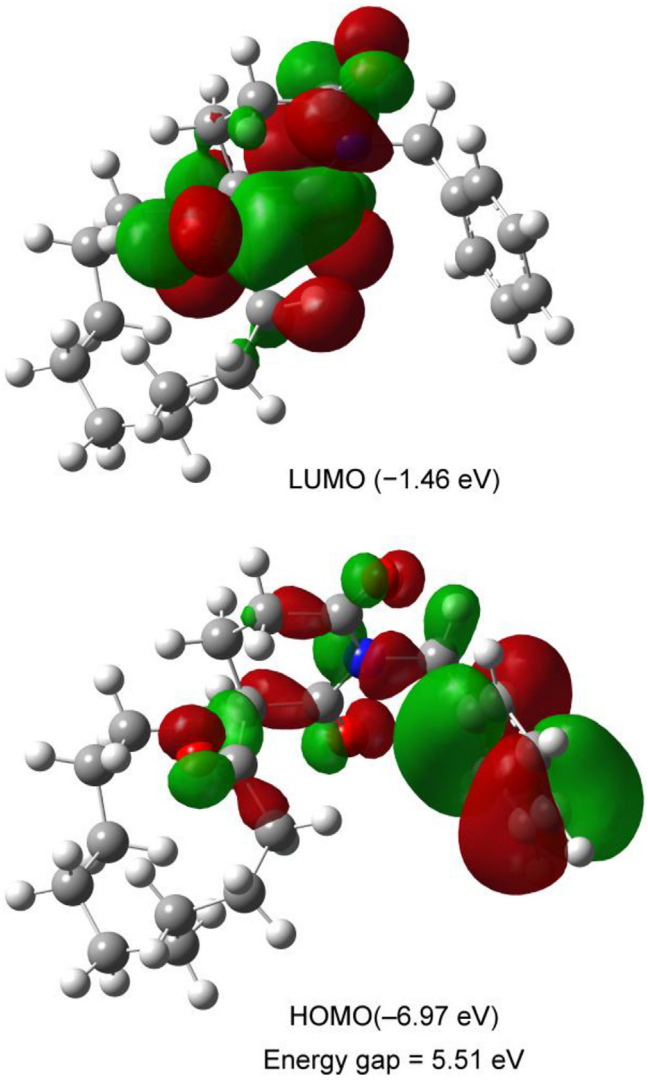

Fig. 7. The frontier molecular orbitals (HOMO and LUMO) for PAH.

Table 4
Theoretical and experimental ^{1}H NMR chemical shifts of PAH compound in $CDCl_3$ solution (atom positions were numbered as in Fig. 2).

Hydrogen	B3LYP/6311++G(d,p)	Experimental
28 H	1.94	1.97
29 H	0.90	0.91
30 H	3.18	3.19
31 H	1.04	1.19
32 H	1.11	1.33
33 H	1.20	1.51
34 H	1.04	1.19
35 H	1.38	1.58
36 H	1.28	1.52
37 H	1.36	1.56
38 H	1.16	1.31
39 H	1.20	1.50
40 H	1.31	1.53
41 H	1.34	1.54
42 H	1.37	1.57
43 H	1.28	1.53
44 H	1.13	1.50
45 H	0.94	0.94
46 H	2.58	1.59
47 H	1.32	1.54
48 H	1.52	2.59
49 H	2.53	2.56
50 H	2.67	2.69
51 H	2.66	2.67
52 H	5.52	5.01
53 H	4.50	4.91
54 H	7.72	7.34
55 H	7.43	7.22
56 H	7.57	7.27
57 H	7.57	7.22
58 H	7.82	7.34

Table 5
Theoretical and experimental ^{13}C NMR chemical shifts of PAH compound in $CDCl_3$ solution (atom positions were numbered as in Fig. 2).

Carbon	B3LYP/6-311++G(d,p)	Experimental
2 C	182.53	171.9
3 C	68.24	59.96
4 C	28.82	23.26
5 C	35.71	29.94
6 C	183.35	172.68
7 C	219.09	204.81
11 C	40.29	34.66
12 C	26.33	21.99
13 C	27.01	23.07
14 C	26.63	22.4
15 C	31.93	26.26
16 C	26.19	21.66
17 C	24.93	21.21
18 C	31.41	26.21
19 C	22.80	18.78
20 C	39.14	33.81
21 C	48.33	43.39
22 C	146.99	136.92
23 C	136.45	128.81
24 C	135.48	128.4
25 C	134.10	127.52
26 C	134.86	128.4
27 C	138.54	128.81

spectra of PAH were recorded in $CDCl_3$ and shown in Figs. S3 and S4 (Supplementary material). The experimental and theoretical values for ^{1}H and ^{13}C NMR shifts of PAH are presented in Tables 4 and 5.

In experimental ^{1}H NMR spectrum of PAH, shifts of aliphatic C-H protons are occurred in the range of 0.91–5.91 ppm and the calculated are in the range 0.90–5.52 ppm. There are many differences in the chemical shifts in the aliphatic region of this spectrum. For example, the chemical shift of hydrogen attached to carbon near the carbonyl group is higher than one that would be expected regarding the electron density around the hydrogen. The hydrogen atom of C11–H30 group appears at higher chemical shift of 3.19 ppm due to influence of carbonyl group C7=O10 with theoretical peak at 3.18 ppm. The same applies for the hydrogens bonded to C20 (H46 and H47) appear at 1.59 and 1.54 ppm due to influence of carbonyl group C2=O9. Two multiple signals appearing at 2.56, 2.59 and 2.67, 2.69 ppm are assigned to protons (H49, H48 and H51, H50) of two methylene groups in glutarimide ring, $C4H_2$ and $C5H_2$ of PAH (Table 4). These signals show good agreement with theoretical values in the region 1.52–2.67 ppm. Two doublets of doublets at 4.91 and 5.01 ppm (in $CDCl_3$ solution) mark the methylene hydrogens H53 and H52 of methylene group $C21H_2$. The calculated chemical shift values for these hydrogen atoms (with respect to TMS) are 4.5 and 5.52 ppm in $CDCl_3$ solution. The calculated chemical shift values for phenyl ring hydrogens are at 7.43–7.82 ppm and experimental peaks for these atoms are in the range of 7.22–7.34 ppm.

Chemical shifts of the carbon atoms in ^{13}C NMR spectra of PAH do not show unexpected values. In the experimental ^{13}C NMR spectrum, carbon atoms of methylene groups of cyclododecanone ring show signals in the range of 18.78–34.66 ppm and correlate very well with the computed values in the range of 22.8–40.29 ppm, Table 5. The methylene carbon atoms of glutarimide ring C4 and C5 appear at 23.26 and 29.94 ppm, and calculated values are 28.82 and 35.71 ppm. Spiro carbon atom C3 is observed at 59.96 ppm, whereas the corresponding computed value is 68.24 ppm. Signals for aromatic carbons are observed in the range 127.52–136.92 ppm for the phenyl ring of PAH. The carbonyl atoms C2, C6 and C7 resonating at 171.9, 172.68 and 204.81 ppm and computed values are 182.53, 183.35 and 219.09 ppm.

4.7. Molecular electrostatic potential (MEP)

Considering the great anticancer activity of PAH molecule, it was necessary to find the molecular fragments that are responsible for this activity as well as for chemical reactivity. The analysis of molecular electrostatic potential could predict those parts of molecule responsible for the electrophilic and nucleophilic reactions as well as inter- and/or intra-molecular bonds. The MEP at the B3LYP/6-311++G(d,p) optimized geometry was calculated and depicted in Fig. 8. The negative regions of the MEP are related to electrophilic reactivity and are colored in red and yellow. The positive, blue regions are related to nucleophilic reactivity, Fig. 8. As can be seen from the figure, negative region is localized over the N and O atoms. The maximum positive region, dark blue, is localized on the C–H

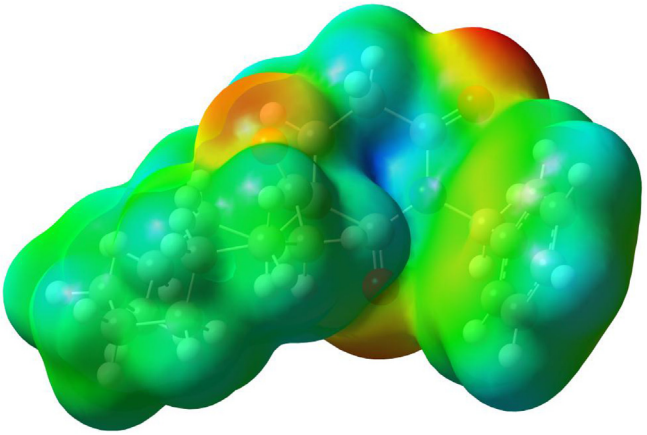

Fig. 8. MEP of investigated molecule calculated with B3LYP/6-311++G(d,p) method.

bonds of glutarimide ring. This region gives information about possible sites for nucleophilic attack. According to these calculated results, the MEP map shows that the negative sites are on electronegative nitrogen atom of the imide group and oxygen atoms of carbonyl groups. The positive sites are around the hydrogen atoms of glutarimide ring.

5. Conclusion

The conformational stability of PAH is thoroughly studied and results are presented in this paper. The most stable conformer of the glutarimide spiro derivative PAH was found and its spectroscopic properties were investigated experimentally and with the help of DFT. The most stable conformer **I** has *cis* orientation of benzyl group and carbonyl group of cyclododecanone ring. The conformational, vibrational, electronic and NMR analyses were done with B3LYP/6-311++G(d,p) method. In addition, NBO analysis has provided evidence of the ICT through the molecule. The MEP map anticipates that imide fragment (oxygen and nitrogen atoms) of PAH is the most reactive site for electrophilic and hydrogen atoms of methylene groups of glutarimide ring for nucleophilic attack.

Acknowledgments

This work has been financially supported by Ministry of Education and Science, Republic of Serbia, under Grant Nos. 172035 and 172032. Numerical simulations were run on the PARADOX cluster at the Scientific Computing Laboratory of the Institute of Physics Belgrade, supported in part by the Ministry of Education, Science and Technological Development of the Republic of Serbia under project No. ON171017.

Appendix A. Supplementary data

Supplementary data associated with this article can be found in the online version, at http://dx.doi.org/10.1016/j.molstruc.2017.02.012. These data include MOL files and InChiKeys of the most important compounds described in this article.

References

[1] F. Matsuda, S. Terashima, Tetrahedron 44 (1988) 4721–4736, http://dx.doi.org/10.1016/S0040-4020(01)86175-5.
[2] J. Ju, S.R. Rajski, S.-K. Lim, J.-W. Seo, N.R. Peters, F.M. Hoffmann, B. Shen, J. Am. Chem. Soc. 131 (2009) 1370–1371, http://dx.doi.org/10.1021/ja808462p.
[3] K. Sugawara, Y. Nishiyama, S. Toda, N. Komiyama, M. Hatori, T. Moriyama, Y. Sawada, H. Kamei, M. Konishi, T. Oki, J. Antibiot. 45 (1992) 1433–1441, http://dx.doi.org/10.7164/antibiotics.45.1433.
[4] A.L. Machado, L.M. Lima, J.X. Araujo Jr., C.A.M. Fraga, V.L.G. Koatz, E.J. Barreiro, Bioorg. Med. Chem. Lett. 15 (2005) 1169–1172, http://dx.doi.org/10.1016/j.bmcl.2004.12.012.
[5] J.B. Bartlett, K. Dredge, A.G. Dalgleish, Nat. Rev. Cancer 4 (2004) 314–322, http://dx.doi.org/10.1038/nrc1323.
[6] Y.-H. Wu, J.W. Rayburn, L.E. Allen, H.C. Ferguson, J.W. Kissel, J. Med. Chem. 15 (1972) 477–479, http://dx.doi.org/10.1021/jm00275a009.
[7] L.B. Barradell, A. Fitton, CNS Drugs 5 (1996) 147–152, http://dx.doi.org/10.2165/00023210-199605020-00006.
[8] T.G. Obrig, W.J. Culp, W.L. McKeehan, B. Hardesty, J. Biol. Chem. 246 (1971) 174–181.
[9] H. Kondo, T. Oritani, H. Kiyota, Eur. J. Org. Chem. 2000 (2000) 3459–3462, http://dx.doi.org/10.1002/1099-0690(200010)2000:20<3459::AID-EJOC3459>3.0.CO;2-F.
[10] R.P. Frohardt, H.W. Dion, Z.L. Jakubowski, A. Rydeer, J.C. French, Q.R. Bartz, J. Am. Chem. Soc. 81 (1959) 5500–5506, http://dx.doi.org/10.1021/ja01529a059.
[11] B.S. Kim, S.S. Moon, B.K. Hwang, J. Agric. Food Chem. 47 (1999) 3372–3380, http://dx.doi.org/10.1021/jf981259s.
[12] D.K.K. Ha, W.H. Lau, Cancer Lett. 41 (1988) 217–224, http://dx.doi.org/10.1016/0304-3835(88)90119-X.
[13] M.I. Andres, P. Sanz, A. Garfia, G. Repetto, M. Repetto, In Vitro Toxicol. 10 (1997) 319–328.
[14] X. Armoiry, G. Aulagner, T. Facon, J. Clin. Pharm. Ther. 33 (2008) 219–226, http://dx.doi.org/10.1111/j.1365-2710.2008.00920.x.
[15] S. Lentzsch, M.S. Rogers, R. LeBlanc, A.E. Birsner, J.H. Shah, A.M. Treston, K.C. Anderson, R.J. D'Amato, Cancer Res. 62 (2002) 2300–2305.
[16] I. Antonini, R. Volpini, D. Dal Ben, C. Lambertucci, G. Cristalli, Bioorgan. Med. Chem. 16 (2008) 8440–8446, http://dx.doi.org/10.1016/j.bmc.2008.08.027.
[17] J.T. Norton, M.A. Witschi, L. Luong, A. Kawamura, S. Ghosh, M.S. Stack, E. Sim, M.J. Avram, D.H. Appella, S. Huang, Anti Cancer Drugs 19 (2008) 23–26, http://dx.doi.org/10.1097/CAD.0b013e3282f00e17.
[18] A. Wu, Y. Xu, X. Qian, J. Wang, J. Liu, Eur. J. Med. Chem. 44 (2009) 4674–4680, http://dx.doi.org/10.1016/j.ejmech.2009.07.011.
[19] M.K. Hargreaves, J.G. Pritchard, H.R. Dave, Chem. Rev. 70 (1970) 439–469, http://dx.doi.org/10.1021/cr60266a001.
[20] J.B. Popović-Djordjević, A.S. Klaus, Ž.S. Žižak, I.Z. Matić, B.J. Drakulić, J. Enzyme Inhib. Med. Chem. 31 (2016) 915–923, http://dx.doi.org/10.3109/14756366.2015.1070844.
[21] J.B. Popović-Đorđević, M.D. Ivanović, V.D. Kiricojević, Tetrahedron Lett. 46 (2005) 2611–2614, http://dx.doi.org/10.1016/j.tetlet.2005.02.087.
[22] R.W. Harrison, J. Comput. Chem. 14 (1993) 1112–1122, http://dx.doi.org/10.1002/jcc.540140911.
[23] A. Pedretti, L. Villa, G. Vistoli, J. Comput. Aid Mol. Des. 18 (2004) 167–173, http://dx.doi.org/10.1023/B: JCAM.0000035186.90683.f2.
[24] W. Humphrey, A. Dalke, K. Schulten, J. Mol. Graph 14 (1996) 33–38, http://dx.doi.org/10.1016/0263-7855(96)00018-5.
[25] M.J. Frisch, G.W. Trucks, H.B. Schlegel, G.E. Scuseria, M.A. Robb, J.R. Cheeseman, G. Scalmani, V. Barone, B. Mennucci, G.A. Petersson, H. Nakatsuji, M. Caricato, X. Li, H.P. Hratchian, A.F. Izmaylov, J. Bloino, G. Zheng, J.L. Sonnenberg, M. Hada, M. Ehara, K. Toyota, R. Fukuda, J. Hasegawa, M. Ishida, T. Nakajima, Y. Honda, O. Kitao, H. Nakai, T. Vreven, J.A. Montgomery Jr., J.E. Peralta, F. Ogliaro, M. Bearpark, J.J. Heyd, E. Brothers, K.N. Kudin, V.N. Staroverov, R. Kobayashi, J. Normand, K. Raghavachari, A. Rendell, J.C. Burant, S.S. Iyengar, J. Tomasi, M. Cossi, N. Rega, J.M. Millam, M. Klene, J.E. Knox, J.B. Cross, V. Bakken, C. Adamo, J. Jaramillo, R. Gomperts, R.E. Stratmann, O. Yazyev, A.J. Austin, R. Cammi, C. Pomelli, J.W. Ochterski, R.L. Martin, K. Morokuma, V.G. Zakrzewski, G.A. Voth, P. Salvador, J.J. Dannenberg, S. Dapprich, A.D. Daniels, Ö. Farkas, J.B. Foresman, J.V. Ortiz, J. Cioslowski, D.J. Fox, Gaussian 09, Revision D.01, Gaussian Inc., Wallingford, CT, 2009.
[26] M.H. Jamróz, Vibrational Energy Distribution Analysis VEDA 4, 2004. Warsaw.
[27] A.P. Scott, L. Radom, J. Phys. Chem. 100 (1996) 16502–16513, http://dx.doi.org/10.1021/jp960976r.
[28] B.J. Orr, J.F. Ward, Mol. Phys. 20 (1970) 513–526, http://dx.doi.org/10.1080/00268977000101521.
[29] R. Ditchfield, J. Chem. Phys. 56 (1972) 5688–5691, http://dx.doi.org/10.1063/1.1677088.
[30] K. Wolinski, J.F. Hinton, P. Pulay, J. Am. Chem. Soc. 112 (1990) 8251–8260, http://dx.doi.org/10.1021/ja00179a005.
[31] M. Cossi, N. Rega, G. Scalmani, V. Barone, J. Comput. Chem. 24 (2003) 669–681, http://dx.doi.org/10.1002/jcc.10189.
[32] E.D. Glendening, A.E. Reed, J.E. Carpenter, F. Weinhold, NBO version 3.1, TCI, University of Wisconsin, Madison, 1998.
[33] V.M. Arsovski, B.Đ. Božić, J.M. Mirković, V.D. Vitnik, Ž.J. Vitnik, S.D. Petrović, G.S. Uśćumlić, D.Ž. Mijin, J. Mol. Mod. 21 (2015) 239, http://dx.doi.org/10.1007/s00894-015-2777-z.
[34] V.D. Vitnik, Ž.J. Vitnik, Spectrochim. Acta A 138 (2015) 1–12, http://dx.doi.org/10.1016/j.saa.2014.11.005.
[35] V.D. Vitnik, Ž.J. Vitnik, N.R. Banjac, N.V. Valentić, G.S. Uśćumlić, I.O. Juranić, Spectrochim. Acta A 117 (2014) 42–53, http://dx.doi.org/10.1016/j.saa.2013.07.099.
[36] V.A. Minaeva, B.F. Minaeva, G.V. Baryshnikov, H. Ågren, M. Pittelkow, Vib. Spectrosc. 61 (2012) 156–166, http://dx.doi.org/10.1016/j.vibspec.2012.02.005.
[37] T.A. Rudol'fi, A.A. Skorubskii, É.B. Krymskaya, J. Appl. Spectrosc. 22 (1975) 1001–1003, http://dx.doi.org/10.1007/BF00608833.
[38] P. Dowd, S.-C. Choi, Tetrahedron 48 (1992) 4773–4792, http://dx.doi.org/10.1016/S0040-4020(01)81574-X.
[39] M. Beer, H.B. Kessler, G.B.B.M. Sutherland, J. Chem. Phys. 29 (1958) 1097–1104, http://dx.doi.org/10.1063/1.1744662.